Available online at www.sciencedirect.com
ScienceDirect
Bioorganic & Medicinal Chemistry 16 (2008) 4064–4074
Bioorganic & Medicinal Chemistry

Modeling and synthesis of novel tight-binding inhibitors of cytochrome P450 2C9

Chi-Chi Peng,[a] Tom Rushmore,[b] Gregory J. Crouch[a] and Jeffrey P. Jones[a,*]

[a]*Department of Chemistry, Washington State University, PO Box 644630, Pullman, WA 99164-4630, USA*
[b]*Department of Drug Metabolism, Merck Research Laboratories, West Point, PA 19486, USA*

Received 16 October 2007; revised 9 January 2008; accepted 14 January 2008
Available online 18 January 2008

Abstract—Cytochrome P450 2C9 (2C9) is one of the three major drug metabolizing cytochrome P450 enzymes in human liver. Although the crystal structure of 2C9 has been solved, the important physicochemical properties of substrate–enzyme interactions remain difficult to be determined. This is due in part to the conformational flexibility of mammalian P450 enzymes. Therefore, probing the active-site with high-affinity substrates is important in further understanding substrate–enzyme interactions. Three-dimensional quantitative structure–activity relationships (3D-QSAR) and docking experiments have been shown to be useful tools in correlating biological activity with structure. In particular we have previously reported that the very tight-binding inhibitor benzbromarone can provide important information about the active-site of 2C9. In this study we report the binding affinities and potential substrate–enzyme interactions of 4H-chromen-4-one analogs, which are structurally similar to benzbromarone. The chromenone structures are synthetically accessible inhibitors and give inhibition constants as low as 4.2 nM, comparable with the very tightest-binding inhibitors of 2C9. Adding these compounds to our previous 2C9 libraries for CoMFA models reinforces the important electrostatic and hydrophobic features of substrate binding. These compounds have also been docked in the 2C9 crystal structure and the results indicate that Arg 108 plays significant roles in the binding of chromenone substrates.

1. Introduction

Cytochrome P450 enzymes (P450) are heme-containing monoxygenases that carry out physiologically important metabolic reactions on endogenous and exogenous substrates. P450 proteins are also important in the oxidation of the majority of clinically prescribed pharmaceuticals. Cytochrome P450 2C9 (2C9) is one of the major isoforms of the cytochrome P450 2C subfamily, responsible for the hepatic clearance of 15% of clinically relevant drugs as the first step in drug clearance.[1] Given that 2C9 makes significant contributions to drug metabolism and is capable of binding a number of compounds with high affinity, it is not surprising that potentially severe drug/drug interactions occur, where co-administered drugs compete for the 2C9 active-site.[2] While the crystal structure of 2C9 with bound warfarin has been solved,[3] kinetic studies with different substrates have given results inconsistent with this structural information.[4–6] Another structure of 2C9 complexed with flurbiprofen at least partially explains this discrepancy by illustrating the importance of conformational flexibility in substrate binding.[7] This conformational flexibility is also evident from site-directed mutagenesis studies.[8] Therefore, further studies on structure–activity relationships may help in accurately predicting substrate–enzyme interactions.

Substrate binding to 2C9 depends on many factors including electrostatic, hydrophobic, and steric properties. Meanwhile, it has been suggested that P450 enzymes have a rather flexible active-site cavity that can undergo conformational changes and affect substrate selectivities for different isoforms.[9] For instance, 2C9 is selective for substrates that are small or moderately sized, lipophilic, and either weakly acidic or neutral.[10,11] Three-dimensional quantitative structure–activity relationships (3D-QSARs) are useful computational techniques for probing the biochemistry of P450s.[12,13] Such approaches can suggest physicochemical descriptors, geometry of structural and functional groups, as well as essential electrostatic, steric, and lipophilicity

Keywords: Cytochrome P450 2C9; Structure–activity relationship; Binding modes; 4H-Chromen-4-one analogs; Drug–drug interactions.
* Corresponding author. Tel.: +1 509 335 5083; fax: +1 509 335 8867; e-mail: jpj@wsu.edu

0968-0896/$ - see front matter © 2008 Elsevier Ltd. All rights reserved.
doi:10.1016/j.bmc.2008.01.021

interactions from substrate conformers. Benzbromarone (Fig. 1), a potent 2C9 inhibitor, has become a model substrate that is used by several research groups including ours to explore structure–function relationships in P450 mediated reactions.[14–19] Our previous study of benzbromarone analogs provides evidence that specific electrostatic and hydrophobic interactions contribute the most to 2C9's specificity.[16] Furthermore, models generated by comparative molecular similarity indices analysis (CoMSIA) suggest that hydrophobicity in 2C9 substrates may be underestimated and that a negative charge is favored at the ketone oxygen rather than the phenol oxygen of benzbromarone analogs.

In this study, we explore a series of novel 4H-chromen-4-one (chromenone) analogs (Fig. 2) which are structural variants of benzbromarone. This new series of compounds contains a variant of the benzofuran ring system in benzbromarone and allows for more facile synthesis of inhibitors with different ring structures. The synthetic route outlined in Scheme 1[20–27] below details the basic ring construction that allows for the chromenone analogs used in this study to probe the active-site of 2C9. Adding these analogs to our prior study using benzbromarone increases our understanding of important substrate–protein interactions and establishes the methodology to explore a number of new structural analogs that bind with high affinity to 2C9.

2. Results

All of our chromenone analogs were synthesized by the routes shown in Scheme 1. Reasonable yields were obtained and the synthetic methods provide a simple route to new 2C9 inhibitors. The inhibition constants for each compound are shown in Figure 2. The inhibition constants range from 4.2 to 6740 nM. Compounds containing halogen atoms adjacent to the phenol oxygen have higher-binding affinity than those without halogens. The diiodo compounds **1**–**3** bind more tightly than the dibromo compound **4**. The tightest-binding compound is compound **3**, which has a propyl side chain at the C-2 position of the chromenone ring, with K_i equal to 4.2 nM. Compounds **1** and **2** contain shorter side chains and bind less tightly with K_i values of 41 and 23 nM, respectively. While compounds with no halogens bound less tightly, compounds **5**–**11** still had inhibition constants that would be a cause of concern with respect to drug/drug interactions since they all bound with a less than 10 μM inhibition constant. Given the high affinity of these compounds, we fit our data to the tight-binding competitive inhibition equation (Eq. 3 presented in the methods section) to determine the K_i values for the tightest-binding compound **3**. No significant change was observed in the inhibition constant since the P450 concentrations in our assays were only 2 nM.

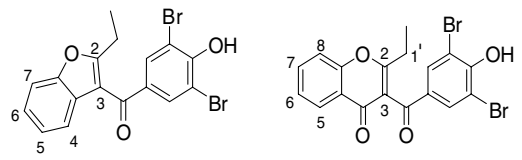

Figure 1. Structural comparison of benzbromarone and a chromenone analogs.

QSAR models were generated by addition of the chromenone analogs in Figure 2 to our previous library of compounds[16,28] along with 14 sulfaphenazole analogs. Models were constructed using just the chromenone subset of the entire library as well as the entire library. When just the 11 chromenone analogs were used, the number of components was limited to three. A total of two training sets were used to construct CoMFA models for inhibition and the results are shown in Table 1. Each training set gave significant models as judged by the cross-validated q^2 values.[29] For the 11 compound library, the CoMFA model gave the steric factor more weight than the electrostatic factor and gave q^2 of 0.836 with ln(standard error) of 0.243. With the 83 compounds and 6 components, the CoMFA model weighted the steric factor and the electrostatic factor equally and gave q^2 of 0.721 with ln(standard error) of 0.822.

When compound **8** was used as a substrate to probe the regioselectivity of a chromenone substrate within the active-site, the O-demethylated metabolite (compound **5**) was found to be the most abundant oxidative metabolite in the reaction and this product was confirmed by spiking the incubation with the metabolite. Two other minor metabolites can be tentatively assigned to aromatic (chromenone aromatic ring) and allylic hydroxylation products. However, due to the low amounts of each metabolite, the metabolites could not be completely characterized. To look at potential-binding modes, compound **8** was subjected to docking to establish potential substrate–enzyme interactions (Fig. 4).

The tightest-binding analog **3** shows no detectable metabolite formation when used as a substrate, presumably due to the slow turnover. However, from the regioselectivity results of compound **8**, we conclude that multiple-binding modes are present; therefore, we may also use autodocking program to simulate the possible binding modes for analog **3**. Out of a total of 3082 poses, these three unique-binding modes shown in Figure 3 reasonably explain the structure–activity relationship for ligand–protein interactions. The other poses reflect minor changes in these three-binding modes.

To look at charge distributions in the tight-binding compounds, density functional calculations were performed on the anionic form of compound **1**. The B3LYP hybrid functional was used with the cc-pVDZ PP basis set with the Stuttgart-Koln MCDHF RSC effective core potential in iodine.[30] Charges were determined by natural population analysis[31] as implemented in Gaussian 2003.[32] The charge on the phenol oxygen was −0.65, the charge on the benzylic carbonyl was −0.60, the charge on the chromenone carbonyl was −0.58, and the charge on the chromenone ring oxygen was −0.53

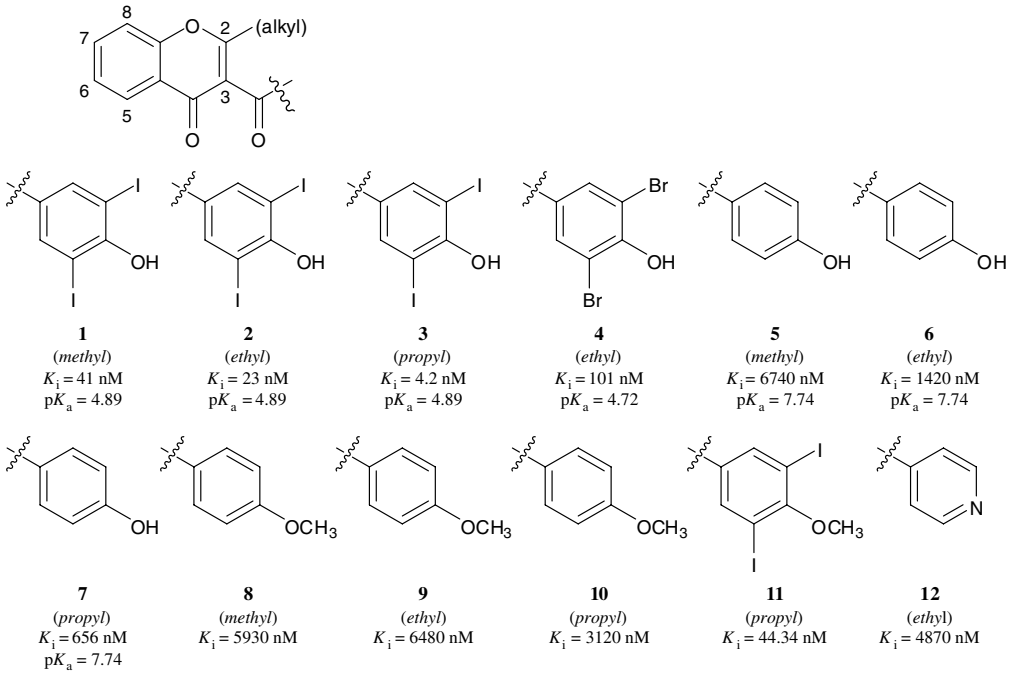

Figure 2. Structures and properties of chromenone analogs used in all models.

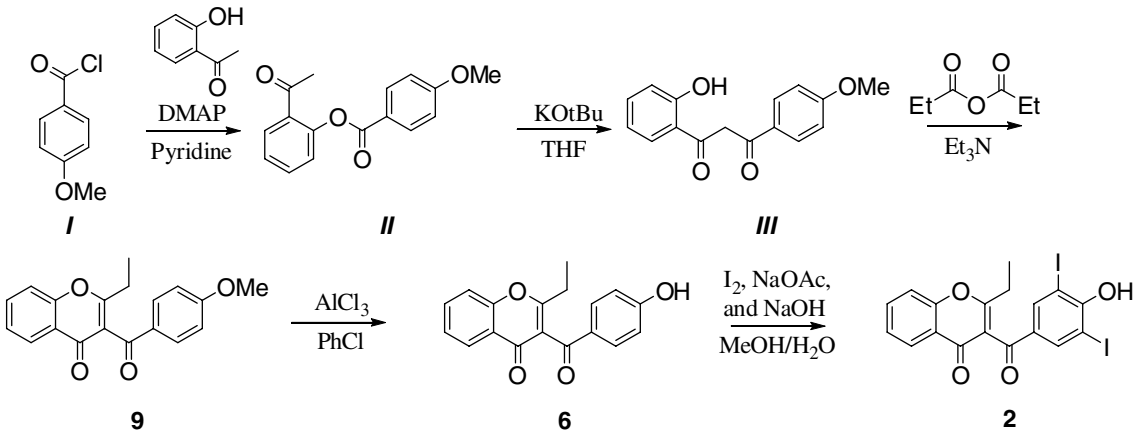

Scheme 1. General synthetic scheme for chromenone analogs.

Table 1. CoMFA model statistics

Descriptor	Fraction steric/electrostatic	q^2	Components	R^2	Standard error (ln)
Chromenones (11 compounds)					
CoMFA					
Steric/electrostatic	0.642/0.358	0.836	3	0.994	0.243
All library (83 compounds)					
CoMFA					
Steric/electrostatic	0.443/0.557	0.721	6	0.893	0.822

(see Structure 1). This even distribution of charge may play a role in the substrates ability' to have multiple-binding orientations. However, this also means that electrostatics is not a major factor determining the strength of binding. This is consistent with the CoMFA results for the chromenones (Table 1), and the relative tight binding of compound **11**.

3. Discussion

Benzbromarone is one of the most potent 2C9 inhibitors with a $K_i < 10$ nM[14] and several of its structural analogs are among the strongest reported inhibitors.[15,16] In prior studies,[15,16] we have shown that combinations of hydrophobic and electrostatic interactions are important

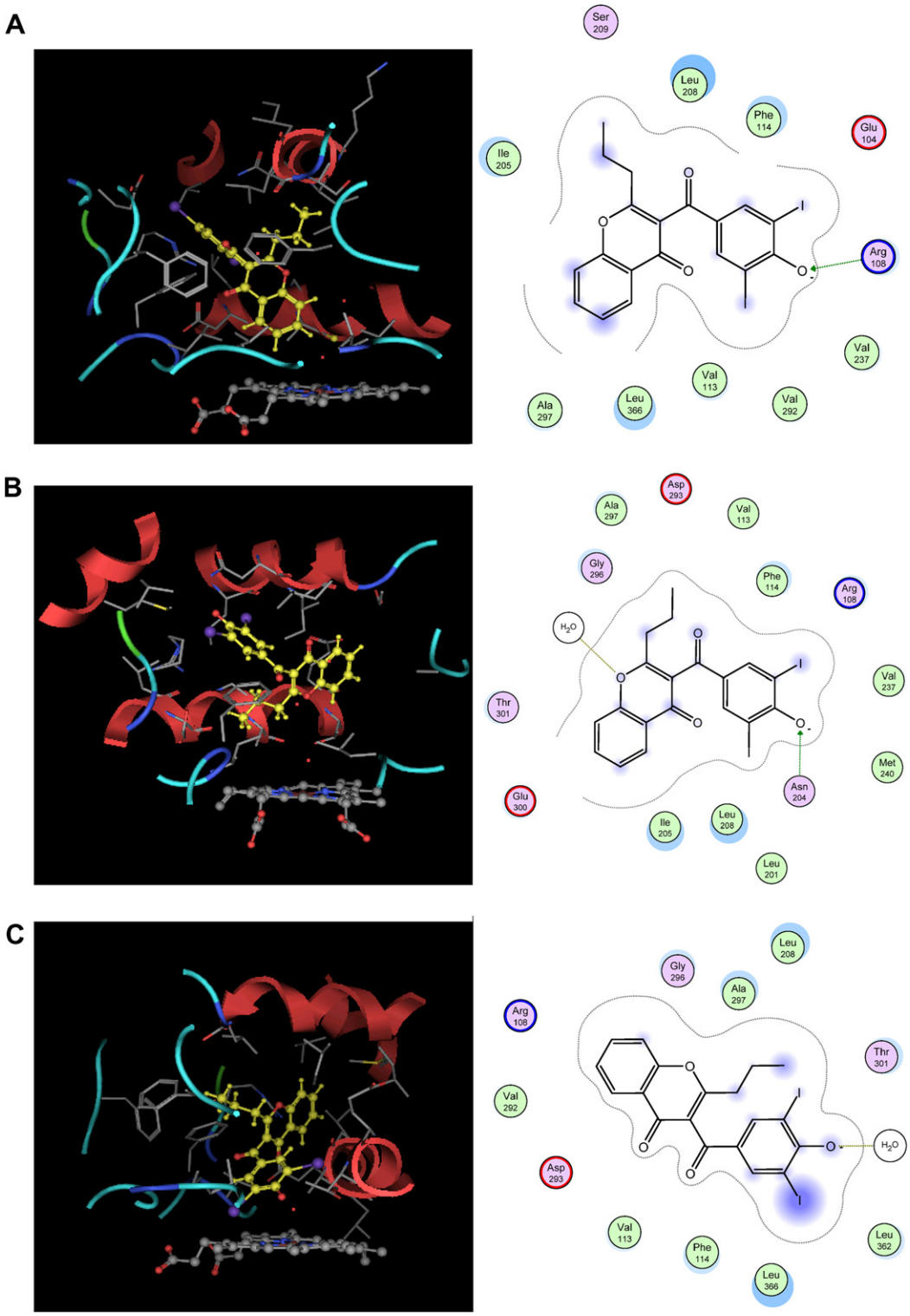

Figure 3. Proposed-binding modes using the flurbiprofen complex of 2C9dH (Protein Data Bank code 1R90). (A) In this mode, Arg 108 can H-bond with the phenol anion and the long side chain at 2 position points toward hydrophobic pocket. (B) The allylic metabolism-binding mode, the phenyl ring faces into the hydrophobic pocket, and the molecule is stabilized by the water network. (C) The third proposed-binding mode would lead to an interaction of the phenolate anion with a water molecule stabilized by Ala 297. On the left is the 3D docking result, on the right is the 2D ligand–residues interaction analysis. The parameters determining the inclusion of protein residues are included in Section 5.

descriptors of 2C9 substrate binding. Both bulky groups on the phenol ring and a negative charge resulting from deprotonation of the phenol oxygen were favored for substrate binding. Meanwhile, the side chain at the C-2 position favored a shorter alkyl group due to steric effects. However, due to the synthetic route, the benzofuran bicyclic ring structure was never varied, and the reason for the unusually tight binding by these struc-

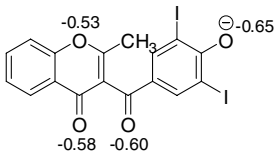

Structure 1. Natural population charges for compound **1**.

tural analogs was not fully elucidated. Here we develop a new synthetic route to high-affinity 2C9 inhibitors containing a 4H-chromen-4-one bicyclic ring system.

These new chromenone analogs (Fig. 2) were used to probe physicochemical properties of substrate–enzyme interaction of 2C9. Given that the chromenone analogs share a phenol moiety with benzbromarones, it is not surprising they share a similar trend in the binding affinity. For example, the iodo chromenones **1**–**3** bind more tightly than the bromo chromenone **4**. This is most likely a result of the increased lipophilicity of the iodine atoms versus bromine atoms when substituted on the phenol ring (estimated log*P* from MOE for compound **2** was 5.667 and for compound **4** was 4.883). Compounds **5**–**11** have no halogen atoms on the phenol ring and their binding affinity is significantly decreased. This suggests the halogens are important in binding.[33,34] For the halogen-substituted chromenones at physiological pH, primarily the phenol should be ionized. Meanwhile, the results also suggest that the active-site has a positively charged residue (Arg 108)[8] that can interact with the negatively charged phenoxide or the negative charged benzylic oxygen via resonance delocalization.[15] This is supported by the idea of an anion-binding region proposed by Smith and Jones in 1992[10] (Structure 2).

The Arg 108 has shown its importance in substrate binding for lipophilic anions from previous studies.[8,7,16] Even though the Arg 108 makes a contribution to binding through electrostatics, the non-anionic compounds, substrate **11** (K_i = 44.34 nM), still show significant high-binding affinity. This suggests that the binding affinity was enhanced by the electrostatic effect but dominated by hydrophobicity. The halogens appear to impact binding due to a combination of lipophilic and electronic effects on ionization (halogens decrease the pK_a of the phenol). However, the hydrophobic effect appears to be dominant as predicted by CoMFA modeling of the 11 compounds (Table 1) which indicates that steric/lipophilic features are twice as important as electrostatic interactions. Therefore, it is a reasonable assumption that in compound **3** the phenol moiety can be positioned to interact with the Arg 108 to have an electrostatic interaction, or it could also interact with the phenyl moiety via π–cation interaction. We can

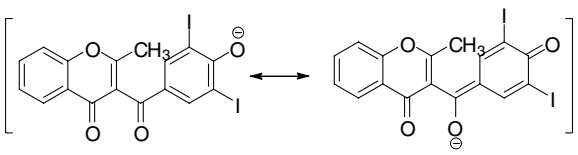

Structure 2. Resonance delocalized anion.

hypothesize from the metabolism of compound **8** and docking results that multiple orientations are possible for all the substrates. However, since no metabolism was observed for compound **3** this cannot be confirmed by metabolic data.

An interesting difference between the chromenones and benzbromarones is the change in affinity as a result of varying the size of the alkyl side chain at the C-2 position (Fig. 1) of the 4H-chromen-4-one or benzofuran fused ring systems. With benzbromarones, we found that binding tightened as the side chain at the C-2 position shortened. However, the opposite trend was observed in this study, with chromenone—compound **3** with a propyl side chain having the highest-binding affinity (K_i = 4.2 nM) of the series. This might be due to the different binding orientation or a separate substrate recognition site.[35] Meanwhile, the increase in lipophilicity from a longer side chain may also be responsible for the tighter binding.

To explore the structure–activity relationship (SAR) in a more quantitative way we included the chromenone analogs in our existing CoMFA model.[16,28] This provided a total of 83 different compounds with diverse structures and binding affinities. When the 3D-QSAR was run with only the chromenones (11 compounds), CoMFA gave models with $q^2 > 0.3$, indicating that significant models could be built even with this small subset of molecules. The CoMFA model for 83 compounds with six components gave a significant model (q^2 of 0.721) with smaller standard errors. CoMFA fields showed steric and electrostatics as contour plot maps which are consistent with the arguments based on visual analysis of the SAR—predicting that negative charges are favored on the phenol group and chromenone C-2 side chain, positive charges are favored near the benzylic carbon, more bulk is favored on the area next to the phenol group, and less bulk on the phenol group itself.

The crystal structure of 2C9 has been solved with both flurbiprofen and warfarin bound.[3,7] To determine if our structure–activity relationships are consistent with the known structures, we docked the tightest-binding compound in the active-site. While warfarin is structurally similar to our chromenone analogs, it has been shown to bind in a site at some distance from the heme iron. This binding mode is not likely to be catalytically competent since the substrate is far removed from the active-oxygen species. Given this binding mode, the possibility of a conformational change in the protein prior to turnover is reasonable. Therefore, we used the flurbiprofen-bound crystal structure for docking.[7] The important role of the hydrophobic pocket and the cationic or hydrogen donor residue region have been documented by several investigators,[12,33,34] and in the flurbiprofen-bound structure, Arg 108 is pointing into the active-site and can act as a positive charge donor for the anions of the acidic chromenones. The amino acid residue Arg 108 is considered to be critical to the catalytic binding of other acidic ligands including nonsteroidal anti-inflammatory drugs (e.g., ibuprofen, flurbiprofen, and diclofenac).[8,36]

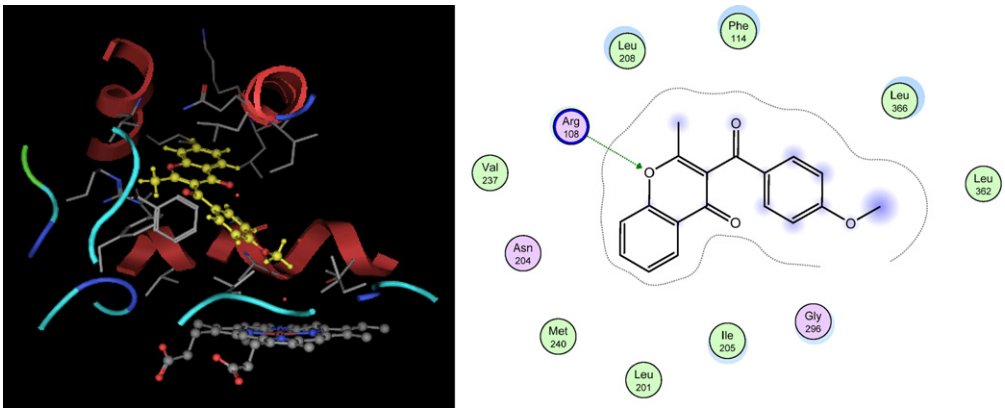

Figure 4. O-Demethylation mode, the methoxy dips toward the heme to provide a catalytic-binding orientation, and the Arg 108 donates its H-bond to pyran oxygen for stabilization.

The autodocking results retain 100 best-scored poses out of 3082 poses. The relative scores for the three-binding modes of the anionic compound **3**, the tightest-binding inhibitor, in Figure 3A–C were numbered as 3, 8, and 63 out of total poses. When anions such as **3** are used as substrates, no significant metabolites are identified by LC/MS (data not shown). Presumably, substrate binding with 2C9 could be dynamic and with multiple-binding modes and this has been shown for warfarin which is metabolized at the 7′ and 4′ positions.[15] Visual analysis of the structures revealed that these three unique orientations are mostly represented by the 100 structures (Fig. 3A–C). Given the propensity of P450 enzymes, including 2C9, to bind in multiple orientations,[37] it is likely that all three-binding modes contribute to the overall inhibition profile.

The first-binding mode of the anionic form of chromenone analog **3** with 2C9 (Fig. 3A) has the phenyl ring facing the Phe 114 to form edge-to-face π-interaction and the C-2 propyl side chain pointing to a hydrophobic pocket comprised of Leu 208, Ser 209, and Ile 205 away from the I-helix. The possible cation interaction results from Arg 108 on the flexible B′-C loop pairing with the anion from the phenol oxygen. The iodine has favorable lipophilic interactions with three valine residues, 113, 292 and 237. Potentially bad substrate–protein interactions include Glu 104, which is close to iodine, and Val 113, which is interacting with the chromenone ring carbonyl oxygen (charge −0.58). This binding mode is supported by the data where the anionic compounds bind with higher affinity and a longer side at the C-2 position enhances this affinity. This binding mode would lead to aromatic oxidation of the chromenone ring.

The second-binding mode would lead to allylic hydroxylation at the 1′ position (Fig. 3B). Binding in this mode is stabilized by the water network linked to Gly 296, Thr 301, and Ala 297, which interact with the charged oxygen (charge −0.53) of the chromenone ring. The phenyl ring is facing the hydrophobic pocket where the phenol oxygen (−0.65) can interact with Asn 204 through nitrogen atom in the side chain, and the iodine can interacts with Phe 114, Val 237, Leu 201, Leu 208 inside the hydrophobic pocket. Potential bad interactions include Arg 108 interacting with the aromatic iodine and Asp 293 interacting with the side chain in the 2 position.

The third proposed binding mode (Fig. 3C) would lead to an interaction of the phenolate anion with a water molecule stabilized by Ala 297. Phe 114 would again interact with the aromatic ring, along with Leu 366 and Leu 362. The side chain at the C-2 position would also be stabilized by hydrophobic interactions. In this mode Arg 108 could have a π–cation interaction with the chromenone ring. Possible bad interactions include Asp 293, which could interact with the chromenone ring and Val 113, which is close to the benzyl carbonyl oxygen with a charge of −0.6.

The site of metabolism can be used to determine possible orientations in the active-site. When compound **8** was used as a substrate to probe the regioselectivity of a oxidation of chromenone substrates within the active-site, the O-demethylated metabolite (compound **5**) was shown to be the most abundant compared to other possible aromatic hydroxylation metabolites. These metabolism studies support the binding mode shown in Figure 3C and the docked structure of **8** in Figure 4. Data show that the binding mode shown in Figures 3C and 4 is likely, at least for uncharged chromenones. In the binding mode shown in Figure 4 Arg 108 has an electrostatic interaction with the chromenone pyran oxygen and the majority of the other interactions are favorable hydrophobic interactions. Since this substrate is not anionic, it could bind in different orientations versus the anionic chromenones.

4. Conclusion

In this study, the chromenone analogs are shown to be potent inhibitors with K_i values as low as 4.2 nM. The 3D-QSAR models with 83 compounds indicate that electrostatics is slightly more important than hydrophobic interactions. Docking studies in the crystal structure of 2C9 indicate multiple-binding modes, similar to our earlier studies with benzbromarone analogs.[37] Since all

the binding modes have favorable electrostatic and hydrophobic interactions, it is possible that the overall tight binding of these compounds arises from multiple partial negative charges that make the molecule highly polarizable, maximizing favorable electrostatic interactions, and minimizing unfavorable interactions. Multiple hydrophobic areas in each analog allow the substrate to have multiple favorable hydrophobic interactions as well.

5. Experimental

5.1. Enzymes, chemicals, and instruments

2C9 Baculosome was prepared as previously described by Rushmore et al.[38] Diclofenac and β-NADPH were purchased from Sigma–Aldrich (St. Louis, MO). HPLC-grade solvents were purchased from EMD Chemicals Inc. and used without purification (Gibbstown, NJ). All other chemicals were purchased from commercial sources and used without purification. The ^{1}H and ^{13}C NMR spectra were gathered on a Varian Mercury Vx 300 MHz spectrometer using TMS as internal standard. A Hewlett Packard 8453 single-beam spectrophotometer with HP 845x UV–visible system was used to determine substrate concentrations. HPLC system was from Agilent 1100 Series with an Alltima C_{18} 5 μm 3.2 × 150 mm column from Alltech. pK_a was estimated using Marvin Applets (ChemAxon Kft. Budapest, Hungary).

5.2. Incubation conditions

Diclofenac was used as a 2C9 substrate and K_i values were determined from the formation rates of 4-hydroxydiclofenac. Four different final concentrations of diclofenac (5, 10, 20, and 30 μM) in 100 mM potassium phosphate buffer at pH 7.4 were used. Three different inhibitor concentrations were added for each of the different concentrations of diclofenac. One picomole of 2C9 Baculosome was added to the incubation mixtures containing the substrate and selected inhibitor and followed by preincubation for 5 min at 37 °C. NADPH was added to a final concentration of 1 mM to initiate the reaction. The final volume of all incubations was 500 μL. Reactions were quenched after 5 min by adding 200 μL of 6% acetic acid in acetonitrile containing an internal standard (0.05 mM phenacetin). The enzyme was removed by centrifugation and product formation was analyzed using HPLC separation UV detection. The HPLC system contained a reverse phase chromatography beginning with 30% of mobile phase A: MeOH and 70% of mobile phase B: (30% acetonitrile: 70% water containing 1 mM perchloric acid) with a linear gradient to 95% of MeOH over 6 min.[39] Each compound's K_i was determined from Eq. 1 using GraphPad Prism4 (San Diego, CA) graphing software.

$$v = \frac{V_m \times [S]}{\left(1 + \frac{[I]}{K_i}\right) K_m + [S]} \quad (1)$$

5.3. K_i determination from IC_{50} measurements

Diclofenac as substrate was used at K_m concentrations to perform the measurement. Inhibitors at three different concentrations were added across to the reaction mixtures containing the same substrate concentration and P450 enzyme (1 pmol). The same incubation procedure and HPLC analysis (detailed above) were used to measure product formation rates. IC_{50} and K_i values were calculated by GraphPad Prism4 graphing software using Eq. 2

$$K_i = \frac{IC_{50}}{1 + \frac{[S]}{K_m}} \quad (2)$$

5.4. Incubation conditions for compound 8 metabolism

Compound **8** was used as a 2C9 substrate. Incubations contained 18 pmol of 2C9 baculosomes, 100 μM substrate **8** and were preincubated for 5 min at 37 °C. NADPH was added to a final concentration of 2 mM to initiate the reaction. The final volume of all incubations was 1 mL. Reactions were quenched after 1 h by adding 200 μL of acetonitrile. The enzyme was removed by centrifugation and supernatant was extracted with ether 1 mL. Product formations were analyzed using HPLC separation and determined by triple quad mass spectrometer (API 4000 LC/MS/MS, Applied Biosystem, MDS Sciex, Toronto, Canada). HPLC used a reverse phase column (Micro-Tech Scientific Inc. C_{18} 5 μm 300 A 150 mm × 1000 μm I.D.) with the mobile phase beginning with 2% of mobile phase A: acetonitrile and 98% of mobile phase B: water with a linear gradient to 70% of acetonitrile over 12 min. The flow rate was 175 μL/min and the *m*/*z* monitored were 281.0 and 311.0 and their fragments. As a result of the low levels of metabolites, no kinetics were done.

5.5. Kinetics of tight-binding inhibitors

Eq. 3 was used to determine the competitive tight-binding inhibitor dissociation constant, K_i, where A is substrate concentration and K_a is the Michaelis constant[40]

$$\frac{I_t}{1 - \frac{v_i}{v_o}} = E_t + K_i \left(\frac{A_t + K_a}{K_a}\right) \frac{v_o}{v_i} \quad (3)$$

5.6. Synthesis of chromenones

All compounds were synthesized by modified literature procedures.[20–27] An example is given with the synthesis of chromenone analog **2**.

5.6.1. Synthesis of 2-acetylphenyl 4-methoxybenzoate (II).[20,21] To a 100 mL round-bottom flask fitted with a stir bar were combined 2-hydroxyl acetophenone (1 g, 7.34 mmol) and anhydrous pyridine (10 mL). This solution was cooled to approximately 0 °C (ice bath) at which point *p*-anisoyl chloride (**I**) (1.378 g, 8.08 mmol) and 4-dimethylaminopyridine (0.08 g, 0.734 mmol) were added. The reaction was allowed to warm to room temperature and stirred for 12 h. The reaction was quenched with a mixture of ice (15 g) and 1 N HCl (aq) 25 mL and

the organic phase was extracted with ethyl acetate and washed with brine (2× 75 mL) and water (2× 75 mL). The organic layer was dried with $MgSO_4$, filtered, and the solvent was removed on a rotary evaporator. The resulting white powder was dissolved in a minimum amount of CH_2Cl_2 and crystallized upon cooling to give white crystals of 2-acetylphenyl 4-methoxybenzoate (**II**) in 76% yield; mp 106–108 °C. ^{1}H NMR ($CDCl_3$) δ 8.17 (d, J = 9 Hz, 2H), 7.85 (dd, J = 1.8, 7.5 Hz, 1H), 7.57 (m, 1H), 7.35 (m, 1H), 7.22 (dd, J = 1.2, 8.4 Hz, 1H), 7.00 (d, J = 8.7 Hz, 2H), 3.89 (s, 3H), 2.54 (s, 3H); ^{13}C NMR ($CDCl_3$) δ 197.96, 165.03, 164.35, 149.76, 133.57, 132.71, 131.72, 130.40, 126.25, 124.21, 121.69, 114.25, 55.79, 30.19.

5.6.2. Synthesis of 1-(2-hydroxyphenyl)-3-(4-methoxyphenyl)propane-1,3-dione (III).[22,25] 2-Acetylphenyl 4-methoxybenzoate (**II**) (0.3 g, 1.11 mmol) was added to a 100 mL round-bottom flask fitted with a stir bar and containing anhydrous THF (30 mL). To this solution, KO^{t}Bu (0.125 g, 1.11 mmol) in THF (5 mL) was added and the round bottom was fitted with a reflux condenser and argon flush and refluxed for 12 h. After this, the solution was cooled to room temperature and the pH of the solution was adjusted to 3 using 3 N HCl (aq). The resulting mixture was concentrated on a rotary evaporator to give a brown oil that was extracted with CH_2Cl_2 (1× 75 mL). The organic layer was isolated and extracted sequentially with 5% sodium bicarbonate (2× 75 mL), water (2× 75 mL) and brine (2× 75 mL). The organic layer was dried with $MgSO_4$, and the solvent was evaporated using a rotary evaporator. The residue was concentrated to oil and crystallized from ethanol to yield yellow needles of 1-(2-hydroxyphenyl)-3-(4-methoxyphenyl)propane-1,3-dione (**III**) in 88% yield; mp 109–111 °C. This compound is without purification in the subsequent step.

5.6.3. Synthesis of 2-ethyl-3-(4-methoxybenzoyl)-4H-chromen-4-one (9).[23] Propanoic anhydride (0.156 g, 1.2 mmol) was combined with 1-(2-hydroxyphenyl)-3-(4-methoxyphenyl)propane-1,3-dione (**III**) (0.3 g, 1.11 mmol) and freshly distilled triethylamine (5 mL) in a 100 mL round-bottom flask fitted with a stir bar and reflux condenser under argon. The mixture was heated to reflux for 12 h. Then, the reaction was cooled to room temperature and directly extracted with ethyl acetate (1× 75 mL). The organic layer was isolated and extracted sequentially with saturated sodium bicarbonate (2× 75 mL), water (2× 75 mL), and brine (2× 75 mL). The organic layer was dried with $MgSO_4$, and the solvent was evaporated using a rotary evaporator. The resulting oil was purified by chromatography (70 g, silica gel 60 0.063–0.200 mm) with (hexanes/ethyl acetate 2:1) and obtained as white crystals of 2-ethyl-3-(4-methoxybenzoyl)-4H-chromen-4-one (**9**) in 87% yield; mp 100–101 °C. ^{1}H NMR ($CDCl_3$) δ 8.18 (dd, J = 1.8, 7.8 Hz, 1H), 7.90 (d, J = 9 Hz, 2H), 7.70 (m, 1H), 7.49 (dd, J = 1.2, 8.4 Hz, 1H), 7.41 (m, 1H), 6.92 (d,J = 9 Hz, 2H), 3.85 (s, 3H), 2.62 (q, J = 7.5 Hz, 2H), 1.29 (t, J = 7.5 Hz, 3H); ^{13}C NMR ($CDCl_3$) δ 192.30, 176.37, 168.99, 164.43, 156.32, 134.19, 132.14, 130.47, 126.21, 125.55, 123.68, 122.80, 118.12, 114.22, 55.77, 26.56, 12.01.

5.6.4. Synthesis of 2-ethyl-3-(4-hydroxybenzoyl)-4H-chromen-4-one (6). In a 100 mL round-bottom flask equipped with a stir bar were combined ammonium chloride (0.390 g, 2.92 mmol), 2-ethyl-3-(4-methoxybenzoyl)-4H-chromen-4-one (**9**) (0.3 g, 0.974 mmol) in chlorobenzene (20 mL). The round-bottom flask was fitted with a condenser and argon purge, refluxed for two hours, and allowed to cool to room temperature. The resulting solution was extracted with CH_2Cl_2 (1× 75 mL). The organic layer was isolated and extracted sequentially with water (2× 75 mL) and brine (2× 75 mL). The organic layer was dried with $MgSO_4$, and the solvent was reduced using a rotary evaporator. The resulting solution of product in chlorobenzene was cooled and product crystals collected using vacuum filtration. This product was further purified by recrystallization from isopropyl ether to give 2-ethyl-3-(4-hydroxybenzoyl)-4H-chromen-4-one (**6**) in 82% yield; mp 211–213 °C. ^{1}H NMR ($CDCl_3$) δ 8.39 (s, 1H), 8.24 (dd, J = 1.8, 8.7 Hz, 1H), 7.77 (m, 1H), 7.62 (d, J = 8.7 Hz, 2H), 7.56 (dd, J = 1.2, 8.4 Hz, 1H), 7.48 (m, 1H), 6.57 (d, J = 8.7 Hz, 2H), 2.66 (q, J = 7.5 Hz, 2H), 1.30 (t, J = 7.5 Hz, 3H); ^{13}C NMR ($CDCl_3$) δ 191.73, 177.53, 170.12, 162.82, 156.54, 134.74, 132.17, 129.03, 126.20, 125.98, 123.34, 122.86, 118.28, 116.14, 26.70, 12.00.

5.6.5. Synthesis of 2-ethyl-3-(4-hydroxy-3,5-diiodobenzoyl)-4H-chromen-4-one (chromenone analog 2).[24] In a 100 mL round-bottom flask equipped with a stir bar were combined 2-ethyl-3-(4-hydroxybenzoyl)-4H-chromen-4-one (**6**) (0.122 g, 0.415 mmol), AcONa·3-H_2O (136 mg, 0.999 mmol), I_2 (253 mg, 0.997 mmol), and MeOH (25 mL). The flask was fitted with a condenser and the solution refluxed 45 min under argon. At this point the reaction was allowed to cool to room temperature at which point NaOH (0.192 M 5 mL, 0.96 mmol) and H_2O (15 mL) were added to the reaction. The reaction was again brought to reflux for an additional 2 h, cooled to room temperature, and stirred for 12 h. The reaction was quenched with an aqueous solution of Na_2SO_3 (2.00 g, 19.41 mmol, 10 mL). The mixture was concentrated on a rotary evaporator and extracted with ethyl acetate (2× 30 mL). The organic layer was isolated and extracted with aqueous HCl (10%, 10 mL), followed by H_2O (1× 10 mL), and brine (1× 30 mL). The organic layer was isolated, dried ($MgSO_4$), and evaporated to give crystals, which were purified by recrystallization from isopropyl ether to give 2-ethyl-3-(4-hydroxy-3,5-diiodobenzoyl)-4H-chromen-4-one (**2**) in 81% yield; mp 224–227 °C. ^{1}H NMR (DMSO) δ 8.23 (s, 2H), 7.99 (dd, J = 1.5, 8.1 Hz, 1H), 7.84 (m, 1H), 7.37 (d, J = 7.5 Hz, 1H), 7.50 (m, 1H), 2.50 (q, J = 7.2 Hz, 2H), 1.19 (t, J = 7.2 Hz, 3H); ^{13}C NMR (DMSO) δ 190.51, 176.07, 169.56, 161.21, 156.43, 141.07, 135.25, 133.07, 126.35, 125.63, 123.52, 121.79, 119.06, 87.10, 26.60, 12.13.

5.6.6. 3-(4-Hydroxy-3,5-diiodobenzoyl)-2-methyl-4H-chromen-4-one (1). Mp 237–240 °C. ^{1}H NMR (DMSO) δ 8.20 (s, 2H), 7.99 (dd, J = 1.5, 8.1 Hz, 1H), 7.84 (m, 1H), 7.68 (dd, J = 0.6, 7.8 Hz, 1H), 7.50 (m, 1H), 2.28 (s, 3H); ^{13}C NMR (DMSO) δ 189.97, 175.15, 165.72, 160.45, 155.64, 140.35, 134.60, 132.36, 125.69, 124.98, 122.78, 121.76, 118.30, 86.40, 18.90.

5.6.7. 3-(4-Hydroxy-3,5-diiodobenzoyl)-2-propyl-4H-chromen-4-one (3). Mp 198–200 °C. ^{1}H NMR (DMSO) δ 8.11 (s, 2H), 8.02 (dd, J = 0.9, 7.8 Hz, 1H), 7.85 (m, 1H), 7.70 (d, J = 8.7 Hz, 1H), 7.51 (m, 1H), 2.50 (t, J = 7.2 Hz, 2H), 1.70 (hex, J = 7.2 Hz, 2H), 0.882 (t, J = 7.2 Hz, 3H); ^{13}C NMR (DMSO) δ 188.07, 175.93, 167.47, 165.23, 156.34, 141.08, 135.14, 128.20, 126.25, 125.69, 123.47, 123.11, 119.02, 89.03, 34.60, 20.74, 14.16.

5.6.8. 3-(3,5-Dibromo-4-hydroxybenzoyl)-2-ethyl-4H-chromen-4-one (4). Mp 197–200 °C. ^{1}H NMR ($CDCl_3$) δ 8.19 (dd, J = 1.5, 8.1 Hz, 1H), 7.99 (s, 2H), 7.74 (m, 1H), 7.52 (dd, J = 0.9, 7.8 Hz, 1H), 7.45 (m, 1H), 2.64 (q, J = 7.8 Hz, 2H), 1.32 (t, J = 7.8 Hz, 3H); ^{13}C NMR ($CDCl_3$) δ 190.39, 176.22, 170.17, 156.32, 154.42, 134.52, 133.76, 132.13, 126.30, 125.89, 123.55, 121.65, 118.20, 110.69, 26.66, 12.09.

5.6.9. 3-(4-Hydroxybenzoyl)-2-methyl-4H-chromen-4-one (5). Mp 270–272 °C. ^{1}H NMR (DMSO) δ 10.54 (s, 1H) 7.99 (dd, J = 1.8, 8.1 Hz, 1H), 7.82 (m, 1H), 7.76 (d, J = 8.7 Hz, 2H), 7.67 (dd, J = 0.6, 8.4 Hz, 1H), 7.49 (m, 1H), 6.83 (d, J = 8.7 Hz, 2H), 2.24 (s, 3H); ^{13}C NMR (DMSO) δ 191.92, 175.71, 164.80, 163.71, 156.29, 135.21, 132.77, 128.85, 126.28, 125.70, 123.38, 118.92, 116.25, 19.40.

5.6.10. 3-(4-Hydroxybenzoyl)-2-propyl-4H-chromen-4-one (7). Mp 206–209 °C. ^{1}H NMR ($CDCl_3$) δ 8.24 (dd, J = 1.5, 8.1 Hz, 1H), 7.96 (s, 1H), 7.76 (m, 1H), 7.64 (d, J = 8.4 Hz, 2H), 7.54 (d, J = 8.1 Hz, 1H), 7.47 (m, 1H), 6.59 (d, J = 8.7 Hz, 2H), 2.62 (t, J = 7.5 Hz, 2H), 1.78 (hex, J = 7.5 Hz, 2H), 0.95 (t, J = 7.5 Hz, 3H); ^{13}C NMR (DMSO) δ 191.92, 175.97, 167.27, 163.72, 156.34, 135.26, 132.77, 128.97, 126.32, 125.66, 123.44, 123.38, 118.99, 116.24, 34.55, 20.71, 14.12.

5.6.11. 3-(4-Methoxybenzoyl)-2-methyl-4H-chromen-4-one (8). Mp 135–136 °C. ^{1}H NMR ($CDCl_3$) δ 8.18 (dd, J = 1.5, 7.8 Hz, 1H), 7.90 (d, J = 9 Hz, 2H), 7.69 (m, 1H), 7.47 (dd, J = 0.6, 8.4 Hz, 1H), 7.41 (m, 1H), 6.92 (d, J = 9 Hz, 2H), 3.85 (s, 3H), 2.36 (s, 3H); ^{13}C NMR ($CDCl_3$) δ 192.31, 176.07, 165.15, 164.45, 156.19, 134.22, 132.15, 130.29, 126.24, 125.60, 123.66, 123.53, 118.08, 114.24, 55.78, 19.33.

5.6.12. 3-(4-Methoxybenzoyl)-2-propyl-4H-chromen-4-one (10). Mp 92–94 °C. ^{1}H NMR ($CDCl_3$) δ 8.19 (dd, J = 1.5, 7.8 Hz, 1H), 7.90 (d, J = 8.7 Hz, 2H), 7.70 (m, 1H), 7.48 (dd, J = 0.6, 8.7 Hz, 1H), 7.41 (m, 1H), 6.93 (d, J = 9 Hz, 2H), 3.86 (s, 3H), 2.58 (t, J = 7.5 Hz, 2H), 1.77 (hex, J = 7.5 Hz, 2H), 0.95 (t, J = 7.5 Hz, 3H); ^{13}C NMR ($CDCl_3$) δ 192.32, 176.34, 168.19, 164.39, 156.27, 134.16, 132.14, 130.52, 126.28, 125.55, 123.70, 123.39, 118.09, 114.20, 55.77, 34.81, 21.07, 14.06.

5.6.13. 3-(3,5-Diiodo-4-methoxybenzoyl)-2-propyl-4H-chromen-4-one (11). Methylated from compound **3**. To a 50 mL round-bottom flask equipped with a stir bar and a water condenser were combined potassium carbonate (15.42 mg, 0.112 mmol), 10 mL acetone, and compound **3** (25 mg, 0.0556 mmol). The reaction mixture was stirred for 30 min at room temperature during which iodomethane (10.42 mL, 0.167 mmol) was added. The reaction mixture was refluxed overnight and the cooled mixture was filtered through a bed of Celite. The solvent was evaporated by rotary evaporator to give clean white product in 99% yield. ^{1}H NMR ($CDCl_3$) δ 8.25 (s, 2H), 8.18 (dd, J = 1.8, 8.1 Hz, 1H), 7.74 (m, 1H), 7.52 (dd, J = 0.6, 8.4 Hz, 1H), 7.45 (m, 1H), 3.90 (s, 3H), 2.58 (t, J = 7.8 Hz, 2H), 1.80 (hex, J = 7.8 Hz, 2H), 0.98 (t, J = 7.2 Hz, 3H); ^{13}C NMR ($CDCl_3$) δ 190.63, 176.15, 169.52, 163.25, 156.25, 141.10, 136.70, 134.53, 126.28, 125.91, 123.55, 122.09., 118.21, 91.11, 61.02, 34.88, 21.22, 14.07. ESI-MS m/z 574.9 (M+1), 233.0 (M−341.9), 215.2 (M−359.7).

5.6.14. 2-Ethyl-3-isonicotinoyl-4H-chromen-4-one (12).[26,27] To a round-bottom flask equipped with a stirrer and condenser were combined isonicotinic acid (1.27 g, 10.36 mmol) and thionyl chloride (30 mL). The reaction was heated to 70 °C for 1 h with stirring. After this, the condenser was removed and an argon stream was used to remove excess thionyl chloride (15 min). The resulting residue was cooled to room temperature and residual thionyl chloride was removed using a rotary evaporator. The solid was dissolved in two portions of ethyl acetate (2× 30 mL) and the resulting solution was evaporated to solid. The crude isonicotinyl chloride was slowly added to a 100 mL round-bottom flask containing 2-hydroxyl acetophenone (1.4 g 10.28 mmol) and pyridine (10 mL) at 0 °C (ice bath). This reaction mixture was stirred at room temperature for 3 h then was poured into a 200 mL beaker containing 15 g of ice. This aqueous solution was adjusted to pH ~ 6 using aq HCl (3 N). The resulting solid was collected by vacuum filtration and washed with ice cold water (20 mL) and dried under high vacuum. This crude compound was purified by chromatography (60 g, silica gel 60, 0.063–0.200 mm) using a 1:1 mixture of hexane/ethyl acetate. Crystallization from methanol gave pure 2-acetylphenyl isonicotinate in 92% yield. From this stock, 482 mg (2 mmol) was added to a 100 mL round-bottom flask fitted with a stir bar and containing pyridine (5 mL) and powered potassium hydroxide (112.2 mg, 2 mmol). This mixture was stirred vigorously at room temperature overnight. The solution was adjusted to pH ~ 6 with 1 M cold aqueous acetic acid. The resulting solid was collected by vacuum filtration and washed with ice cold water (2× 10 mL). The resulting solid was purified by crystallization from methanol to give 41.5% yield of 1-(2-hydroxyphenyl)-3-(pyridin-4-yl)propane-1,3-dione. Cyclization was performed as for 2-ethyl-3-(4-methoxybenzoyl)-4H-chromen-4-one (**9**) to give a 43.2% yield of 2-ethyl-3-isonicotinoyl-4 H-chromen-4-one (**12**). ^{1}H NMR ($CDCl_3$) δ 8.80 (d, J = 5.4 Hz, 2H), 8.15 (dd, J = 1.5, 8.1 Hz, 1H), 7.74 (m, 1H), 7.67 (d, J = 5.7 Hz, 2H), 7.53 (dd, J = 1.5, 10.2 Hz, 1H), 7.44 (m, 1H), 2.70 (q, J = 7.8 Hz, 2H), 1.35 (t, J = 7.8 Hz, 3H); ^{13}C NMR ($CDCl_3$) δ 193.97, 176.34, 171.66, 156.23, 151.08, 143.56, 134.67, 126.09, 126.03, 123.54, 122.04, 121.39, 118.23, 26.56, 12.23. ESI-MS m/z 280.5 (M+1).

5.6.15. Alignment and comparative molecular field analysis (CoMFA) modeling. Ligands were constructed in SYBYL version 6.6 (Tripos Inc., St. Louis) and minimized using the AM1 semiempirical method in MOPAC. The partial charges of each ligand were

calculated by MNDO as described previously.[16] All the chromenone compounds were aligned with benzbromarone through the phenol rings and the benzylic carbon. Slight changes in the torsion angles of the sp^2 carbonyl were adjusted to make the pyran ring parallel to the furan ring. The pK_i values (biological activity) were used against various descriptors to generate QSAR models. All the models were obtained using defaulted 2.0 cal/mol column filtering for CoMFA. Leave-one-out cross validation was used in each case for the partial least-squares algorithm to determine the optimal number of components. The cross-validated correlation coefficient q^2 was considered significant when it exceed 0.3[29] and a higher q^2 value suggested better predictive ability.

5.7. Automated docking

Substrates were docked into the crystal structure of 2C9 1R90[7] using MOE 2006.08 (Chemical Computing Group Inc. Montreal, Quebec, Canada). Compounds were sketched and underwent energy minimization as entries. Selected substrates were then fitted into the active-site cavity using the automatic docking program, exploring the conformational space associated with each rotatable bond. The parameters were as follows: receptor—receptor atoms; site—selected atoms (glycerol + flurbiprofen); ligand—sketched substrates; placement—alpha triangle; scoring—London dG; retain—100. The parameters for inclusion of the residues by ligand interaction calculations in MOE were fields of H-bond, ionic, and solvent with minimum score of 10%, prospectively. Only the substrate and amino acid residues within 4.5 Å were allowed during the determination. The protein was frozen when the autodocking was performed. The water molecules were modeled before docking them in the crystal structure. Out of the 100 best scoring conformations three unique-binding orientations emerged from this analysis. Compound **8** and anionic form of compound **3** were subjects for docking. The binding modes shown in Figures 3 and 4 were energy minimized. The force field for both docking and energy minimization were Hamiltonian—MMFF94x in MOE.

Acknowledgment

This work was supported by National Institutes of Health Grant No. GM032165.

References and notes

1. Evans, W. E.; Relling, M. V. *Science* **1999**, *286*, 487.
2. Miners, J. O.; Birkett, D. J. *Br. J. Clin. Pharmacol.* **1998**, *45*, 525.
3. Williams, P. A.; Cosme, J.; Ward, A.; Angove, H. C.; Vinkovic, D. M.; Jhoti, H. *Nature* **2003**, *424*, 464.
4. Korzekwa, K. R.; Krishnamachary, N.; Shou, M.; Ogai, A.; Parise, R. A.; Rettie, A. E.; Gonzalez, F. J.; Tracy, T. S. *Biochemistry* **1998**, *37*, 4137.
5. Hutzler, J. M.; Hauer, M. J.; Tracy, T. S. *Drug Metab. Dispos.* **2001**, *29*, 1029.
6. Rettie, A. E.; Eddy, A. C.; Heimark, L. D.; Gibaldi, M.; Trager, W. F. *Drug Metab. Dispos. Biol. Fate Chem.* **1989**, *17*, 265.
7. Wester, M. R.; Yano, J. K.; Schoch, G. A.; Yang, C.; Griffin, K. J.; Stout, C. D.; Johnson, E. F. *J. Biol. Chem.* **2004**, *279*, 35630.
8. Dickmann, L. J.; Locuson, C. W.; Jones, J. P.; Rettie, A. E. *Mol. Pharmacol.* **2004**, *65*, 842.
9. Ortiz de Montellano, P. R. *Cytochrome P450: Structure, Mechanism, and Biochemistry*, 2nd ed.; Plenum: New York, 1995.
10. Smith, D. A.; Jones, B. C. *Biochem. Pharmacol.* **1992**, *44*, 2089.
11. Mancy, A.; Broto, P.; Dijols, S.; Dansette, P. M.; Mansuy, D. *Biochemistry* **1995**, *34*, 10365.
12. Jones, J. P.; He, M.; Trager, W. F.; Rettie, A. E. *Drug Metab. Dispos. Biol. Fate Chem.* **1996**, *24*, 1.
13. de Groot, M. J. *Drug Discovery Today* **2006**, *11*, 601.
14. Takahashi, H.; Sato, T.; Shimoyama, Y.; Shioda, N.; Shimizu, T.; Kubo, S.; Tamura, N.; Tainaka, H.; Yasumori, T.; Echizen, H. *Clin. Pharmacol. Ther.* **1999**, *66*, 569.
15. Locuson, C. W.; Wahlstrom, J. L.; Rock, D. A.; Rock, D. A.; Jones, J. P. *Drug Metab. Dispos. Biol. Fate Chem.* **2003**, *31*, 967.
16. Locuson, C. W.; Rock, D. A.; Jones, J. P. *Biochemistry* **2004**, *43*, 6948.
17. Locuson, C. W.; Wahlstrom, J. L. *Drug Metab. Dispos.* **2005**, *33*, 873.
18. Hummel, M. A.; Locuson, C. W.; Gannett, P. M.; Rock, D. A.; Mosher, C. M.; Rettie, A. E.; Tracy, T. S. *Mol. Pharmacol.* **2005**, *68*, 644.
19. Locuson, C. W.; Gannett, P. M.; Tracy, T. S. *Arch.of Biochem. Biophys.* **2006**, *449*, 115.
20. Cummings, R. T.; DiZio, J. P.; Krafft, G. A. *Tetrahedron Lett.* **1988**, *29*, 69.
21. Kahnberg, P.; Lager, E.; Rosenberg, C.; Schougaard, J.; Camet, L.; Sterner, O.; Nielsen, E. O.; Nielsen, M.; Liljefors, T. *J. Med. Chem.* **2002**, *45*, 4188.
22. Ares, J. J.; Outt, P. E.; Kakodkar, S. V.; Buss, R. C.; Geiger, J. C. *J. Org. Chem.* **1993**, *58*, 7903.
23. Huffman, K. R.; Loy, M.; Ullman, E. F. *J. Am. Chem. Soc.* **1965**, *87*, 5417.
24. Wendt, B.; Ha, H. R.; Hesse, M. *Helv. Chim. Acta* **2002**, *85*, 2990.
25. Bowden, K.; Chehel-Amiran, M. *J. Chem. Soc. Perkin Trans. 2* **1986**, *12*, 2039.
26. Begley, W. J., U.S. Patent Documents 6,201,125 2001.
27. Devitt, P. F.; Timoney, A.; Vickars, M. A. *J. Org. Chem.* **1961**, *26*, 4941.
28. Rao, S.; Aoyama, R.; Schrag, M.; Trager, W. F.; Rettie, A.; Jones, J. P. *J. Med. Chem.* **2000**, *43*, 2789.
29. Cramer, R. D., III; Patterson, D. E.; Bunce, J. D. *J. Am. Chem. Soc.* **1988**, *110*, 5959.
30. Peterson, K. A.; Figgen, D.; Dolg, M.; Stoll, H. *J. Chem. Phys.* **2007**, *126*, 124101.
31. Reed, A. E.; Curtiss, J. L.; Weinhold, F. *Chem. Rev.* **1988**, *88*, 899.
32. Frisch, M. J. T.; Trucks, G. W.; Schlegel, H. B.; Scuseria, G. E.; Robb, M. A.; Cheeseman, J. R.; Montgomery, J. A., Jr.; Vreven, T.; Kudin, K. N.; Burant, J. C.; Millam, J. M.; Iyengar, S. S.; Tomasi, J.; Barone, V.; Mennucci, B.; Cossi, M.; Scalmani, G.; Rega, N.; Petersson, G. A.; Nakatsuji, H.; Hada, M.; Ehara, M.; Toyota, K.; Fukuda, R.; Hasegawa, J.; Ishida, M.; Nakajima, T.; Honda, Y.; Kitao, O.; Nakai, H.; Klene, M.; Li, X.; Knox, J. E.; Hratchian, H. P.; Cross, J. B.; Bakken, V.; Adamo, C.; Jaramillo, J.; Gomperts, R.; Stratmann, R. E.; Yazyev, O.; Austin, A. J.; Cammi, R.; Pomelli, C.; Ochterski, J. W.; Ayala, P. Y.; Morokuma, K.; Voth, G. A.; Salvador, P.; Dannenberg, J. J.; Zakrzewski, V. G.; Dapprich, S.; Daniels, A. D.; Strain, M. C.; Farkas, O.; Malick, D. K.;

Rabuck, A. D.; Raghavachari, K.; Foresman, J. B.; Ortiz, J. V.; Cui, Q.; Baboul, A. G.; Clifford, S.; Cioslowski, J.; Stefanov, B. B.; Liu, G.; Liashenko, A.; Piskorz, P.; Komaromi, I.; Martin, R. L.; Fox, D. J.; Keith, T.; Al-Laham, M. A.; Peng, C. Y.; Nanayakkara, A.; Challacombe, M.; Gill, P. M. W.; Johnson, B.; Chen, W.; Wong, M. W.; Gonzalez, C.; Pople, J. A.; Gaussian, Inc.: Wallingford CT, 2004.

33. Ekins, S.; Bravi, G.; Binkley, S.; Gillespie, J. S.; Ring, B. J.; Wikel, J. H.; Wrighton, S. A. *Drug Metab. Dispos.* **2000**, *28*, 994.
34. de Groot, M. J.; Alex, A. A.; Jones, B. C. *J. Med. Chem.* **2002**, *45*, 1983.
35. Gotoh, O. *J. Biol. Chem.* **1992**, *267*, 83.
36. Johnson, E. F. *Drug Metab. Dispos.* **2003**, *31*, 1532.
37. Locuson, C. W.; Suzuki, H.; Rettie, A. E.; Jones, J. P. *J. Med. Chem.* **2004**, *47*, 6768.
38. Rushmore, T. H.; Reider, P. J.; Slaughter, D.; Assang, C.; Shou, M. *Metab. Eng.* **2000**, *2*, 115.
39. BD. BD Biosciences: San Jose, CA USA, 2005; Vol. 2005.
40. Henderson, P. J. F. *Biochem. J.* **1972**, *127*, 321.